Science Arts & Métiers (SAM)

is an open access repository that collects the work of Arts et Métiers ParisTech researchers and makes it freely available over the web where possible.

To cite this version :

A numerical method to calculate the Abbott parameters:
A wear application

M. Bigerelle[a,b], A. Iost[b,*]

[a]*Laboratoire Roberval, FRE 2833, UTC/CNRS, Centre de recherches de Royallieu BP20529, 60205 Compiègne, France*
[b]*Laboratoire de Métallurgie Physique et Génie des Matériaux, Equipe CPP, ENSAM, USTL, CNRS, 8 Boulevard Louis XIV, 59046 Lille, France*

Abstract

A numerical technique was proposed to plot the Abbott curve and to compute its associated parameters defined by the DIN 4776 and ISO 13565 norms. These parameters were then extended and applied to non-sigmoid Abbott curves. By studying the discretisation errors, we show that a minimum of 200 intercepts, with parabolic interpolations between discretised data profiles, have to be taken into consideration to calculate the parameters as accurately as possible. Experimental profiles were eroded by means of a numerical wear model, and it was shown that the Abbott parameters correlate well with the wear model parameters. Our numerical estimations of Abbott parameters were performed for electro-eroded, tool machined, polished, worn and sandblasted surfaces. Manual measures were compared with our algorithmic method and it was shown that the difference is lower than 1% for *Mr1* and *Mr2* Abbott parameters, but the numerical technique leads to a lower dispersion.

Contents

*Corresponding author. Tel.: +33 3 2062 2233; fax: +33 3 2062 2957.
E-mail address: alain.iost@lille.ensam.fr (A. Iost).

1. Introduction

The Abbott curves [1] are usually used to quantify wear phenomena such as lubricant influence, bearing materials [2] or surface texture [3]. The roughness parameters computed from these curves are defined by the DIN 4776 norm [4] superseded by ISO 13565 [5]. The present development of methods (spectral, fractal, wavelet *et al*) and their implantation led us to connect a computer to roughness profilometers and to compute numerical estimations of the roughness parameters. This way, we developed an algorithm to plot the Abbott curve and to compute the norm parameters. The discretisation of the Abbott curves is studied and the efficiency of the algorithm is tested on various kinds of profiles.

2. The Abbott curves

First, we briefly report on the Abbott roughness parameters defined by the DIN 4776 and the ISO 13565 normalisation.

2.1. Asperities' height distribution

Asperities' height distribution (AHD) is the ratio (in percentage) between the length intercepted by the roughness profile and the scan length L (Fig. 1) at a given height, called c ($c \in [R_{min}, R_{max}]$ where R_{min} is the minimal amplitude of the profile and R_{max} is the maximal one), from the reference line which is the least square line of the profile:

$$\mathrm{AHD}(c) = 100 \sum_i (L_i/L), \qquad (1)$$

where $L_i(c)$ are all the segments of the intersection of the profile $y = f(x)$ with the intercept $y = c$. The Abbott curve is finally obtained by plotting c versus $\mathrm{AHD}(c)$. An example is

presented in Fig. 2(a) for an experimental electro-eroded profile and Fig. 2(b) for its related Abbott curve.

2.2. The Abbott curve parameters

Parameters computed from the Abbott curves are represented in Fig. 2b. Let $F(x)$ be the equation of the straight line that best adjusts the linear part of the Abbott curve, and let us define c_1 and c_2 by $c_1 = F(0)$ and $c_2 = F(100)$. Finally, let us denote by $A(x)$ the Abbott curve equation and by $A^{-1}(x)$ its reciprocal application. The Abbott parameters are defined in Table 1. All these parameters depend on the $F(x)$ equation that represents the best-fitted line calculated in the "linear part" of $A(x)$. The main problem consists in finding the interval $[a,b]$ where $A(x)$ could be considered as linear.

2.3. Remarks on the ISO 13565 normalisation

The Abbott curves correspond exactly to $1-f(x)$, where f is the cumulative density function (CDF) of surface height, provided the profiles are considered as a continuous function. However, for a discretised profile, the results could be different according to the method used to calculate the length intercepted by the roughness profile and the intercepted length c. It will be then judicious to use some parametric estimations (like maximal likelihood estimation), if a probability density function (PDF) cannot be rejected, or a non-parametric one (like kernel density) to estimate the CDF in the other cases. The norm specifies that a straight line must be fitted to the central line of the PDF corresponding to a 40% interval length. No mathematical or statistical justification was given for this interval range. To obtain a linear Abbott curve in the whole interval meaning that $A(x) = F(x) = \alpha$
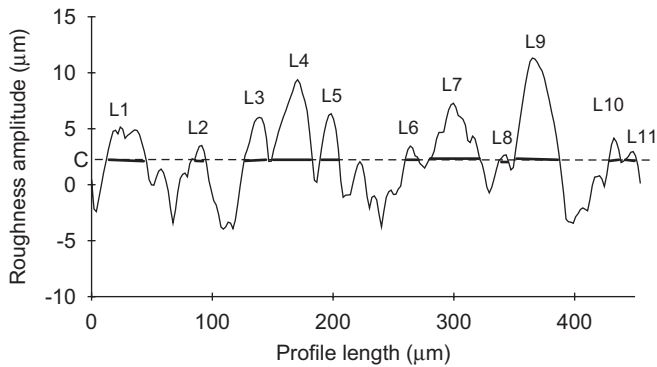
Fig. 1. Roughness profile and description of the method used to plot the Abbott curve from the DIN 4776 or ISO 13565 norms.
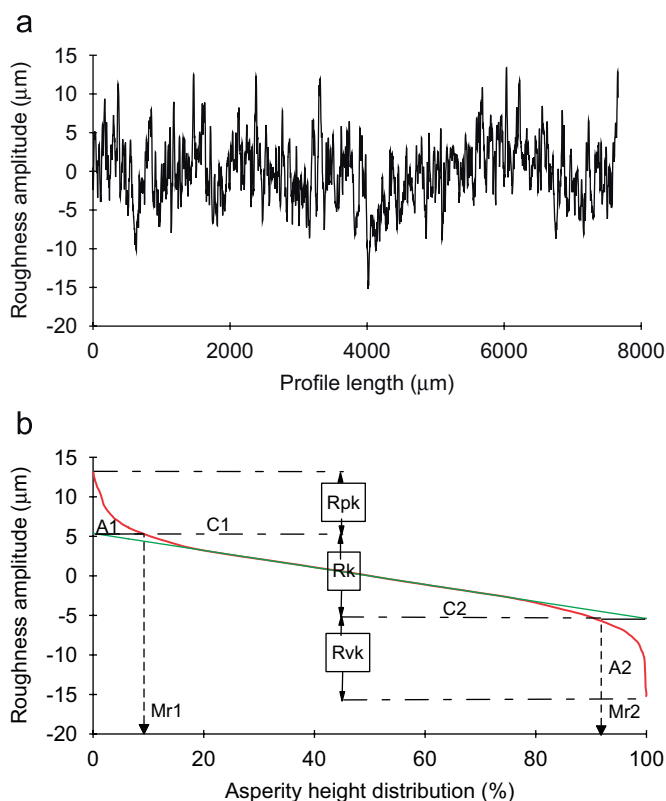

a

b

Fig. 2. An electro-eroded profile obtained by a tactile profilometer (a) and the corresponding curve with definitions of the DIN 4776 or ISO 13565 norms parameters (b).

Table 1
Definition of Abbott parameters

	Definition	Formula	
$A1$	Quantity of solid peaks	$A1 = \int_0^{A^{-1}(c_1)} (A(x) - c_1)\,\mathrm{d}x$	(2)
$A2$	Quantity of solid valleys	$A2 = \int_{A^{-1}(c_2)}^{100} (A(x) - A(100))\,\mathrm{d}x$	(3)
$Mr1$	Threshold as the minimal AHD	$Mr1 = A^{-1}(c_1)$	(4)
$Mr2$	Threshold as the maximal AHD	$Mr2 = A^{-1}(c_2)$	(5)
R_k	Kernel or core roughness depth	$R_k = c_1 - c_2$	(6)
R_{pk}	"Reduced" height peak amplitude	$R_{pk} = A(0) - c_1$	(7)
R_{vk}	"Reduced" height valley amplitude	$R_{vk} = c_1 - A(100)$	(8)
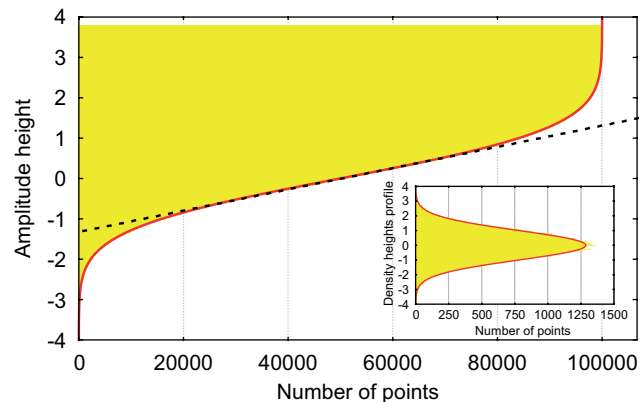
Fig. 3. Gaussian cumulative density function (CDF) of a simulated Gaussian profile discretised in 100 000 points. The curve represents the Gaussian theoretical CDF and the straight line the 40% linear part calculated from ISO 13565 norm. The histogram represents the PDF of the profile height.

$x + \beta$ $\forall x \in [0, 100]$, the stationary signal has to be a triangular one mathematically speaking. The domain of the linear assumption can then be characterised as an amplitude range where roughness can be approached by a triangular signal. If we suppose that the amplitude signal gets a Gaussian PDF (the most current PDF met in tribology), then no linear part exists in the Abbott curve. However, the linear assumption can be a good approximation over a wide range. To visualise the results of the approximation, a Gaussian profile (discretised in 100 000 points) is simulated, the CDF is calculated and then the linear part is plotted according to the ISO 13565 norm. As can be shown in Fig. 3, the central linear part is a good approximation of the real PDF on the 40% interval length. This approximation can be justified by the following remarks:

- A linear relation is no unreasonable approximation for the CDF central parts.
- The central part represents the maximal mass of the material and a linear relation could involve mathematical simplifications of wear models (or more generally physical models) based on the interaction of the surface with a physical process [6,7].

3. Materials, surface machining and roughness recording

To test whether our algorithm holds or not, surfaces were machined using various processes.

3.1. Electro-erosion

35NC16 steel sheets (0.35% C, 4% Ni, Cr) were cut by electro erosion. All process parameters were unchanged except for the pulse times, which are, respectively, 1.5 and 2.5 m s for samples (el_a) and (el_b). Profiles were recorded

using a mechanical stylus profilometer with 8 mm working length discretised in 8000 points.

3.2. Turning

Ten 35NCD4 steel sheets (0.35% C, 1% Ni, Cr, Mo) were machine-turned through the following process: five with a feed rate of 0.1 mm/rev (U_a) and five with a feed rate of 0.35 mm/rev (U_b). Twenty profiles were recorded perpendicular to the grooves using a mechanical stylus profilometer with 4 mm working length discretised in 8000 points.

3.3. Shot peening

Tin base samples (0.95% Sn, 0.05% Sb) E5 were sandblasted (53/106 μm) under two different environmental conditions: E2 in dry environment and E3 in humid environment. Thirty profiles chosen at random were recorded from each sample using a mechanical stylus profilometer with 4 mm working length discretised in 8000 points.

3.4. Wear

Two regions of a Ti-6Al-4V hip prosthesis head, explanted from a human body after 10 years, were named TF (part of the prosthesis where friction is higher) and TB (lower friction area). Using a scanning confocal microscope. 280 profiles were recorded The 85 μm scaling length is discretised in 800 points.

3.5. Grinding

Ti-6Al-4V samples were polished using carborundum disks 80 (P80), 1200 (P1200) or 4000 (P4000). The roughness was recorded using a mechanical stylus profilometer with 4 mm working length discretised in 8000 points.

4. Results and discussion

4.1. Determination of parameters

4.1.1. Principle
The algorithm used to calculate the linear part of the Abbott curve, $F(x)$, could be summed up by five steps:

(i) A minimal set of adjacent points of $A(x)$ is chosen to calculate $F(x)$.
(ii) Linear least-square adjustment is computed.
(iii) Slope precision is quantified by using an appropriate statistical method (Student's confidence interval).
(iv) An adjacent point is further added and steps (ii), and (iii) are reiterated.
   All configurations are tested to find the set of points that leads to the best regression coefficient slope:
(v) The Abbott parameters are calculated.

4.1.2. The Abbott curves' linear part
4.1.2.1. Linear least-square methods (LLSM). Let n be the number of points of the Abbott curve, x_i the abscissa (in percentage) of the ith point and y_i its ordinate (asperity height). The coefficients a and b of the equation $F(x) = a + bx$ were calculated by the linear-least square method with a residual variance s^2 given by

$$s^2 = \sum_{i=1}^{n}(y_i - y_i')^2/n - 2,\qquad(9)$$

where $y_i' = a + bx_i$ are the predicted values and the slope variance estimator s_b^2 is given by

$$s_b^2 = s^2/\sum_{i=1}^{n}(x_i - \bar{x})^2,\qquad(10)$$

where $\bar{x} = \sum_n(x_i/n)$. Following the Gauss–Markov hypotheses [8] and if the residual $y_i - y_i'$ obeys a Gaussian PDF, the random value $(b-\beta)/s_b$ (where β is the unknown value of the slope and s_b its standard deviation) obeys a Student PDF with $\upsilon = n - 2$ degrees of freedom. The confidence interval of the slope at the $1-\alpha$ level is defined by

$$b - t_{1-\alpha/2,n-2}s_b \leqslant \beta \leqslant b + t_{1-\alpha/2,n-2}s_b,\qquad(11)$$

where $t_{x,k}$ is the fractile of the Student PDF with k degrees of freedom and α the significant level of x.

4.1.2.2. Analysis of the LLMS. Eq. (11) is only theoretically valid if the Gauss–Markov hypotheses are not violated and if the residual follows a Gaussian PDF. It can be shown that the Gauss–Markov hypotheses are not respected, meaning that the LLSM method cannot formally be applied. However, using the Bootstrap regression, it can be shown that these violations do not affect the determination of the linear part of the Abbott curve. The values of the coefficients a and b of the straight line are unaffected; so are the Abbott parameters. Then, the LLSM method can be applied without any restriction.

4.1.3. Algorithm
Let M be the number of intercepts used to calculate the asperities' height distribution. Let b_{x_i,x_j} with $x_i < x_j$ be the slope obtained by regression analysis using the set of points $((x_i, y_i), (x_{i+1}, y_{i+1}), \ldots, (x_j, y_j))$ with $i \in [1, M(1 - w)]$ and $j \in [i + 1, Mw]$ where w ($w \in [0..1]$) represents the minimal ratio of adjacent points used to calculate the slope. In the case of the ISO Norm, $w = 0.4$ meaning that 40% of the interpolated line will be used to compute $F(x)$. (This ratio imposes a minimal critical length to avoid detection of abnormal small linear part.) All the configurations b_{x_i,x_j} are computed with their confidence intervals and the "best" slope is obtained when the range of confidence interval (Eq. (11)) is minimised.

Remark. as an adjacent point is added or deleted during this algorithm, it is possible to optimise the computation time by using a recursive method to calculate the regression equation.

4.1.4. Intercept calculation related to the Abbott curves

The intercepted length L_l can be defined by the following set of points:

$$L_l = \{(x_l, y_l), (x_k, y_k), x_k > x_l/y_l = c,$$
$$y_k = c, y_i > c; i \in [l+1..k-1]; L_l = x_k - x_l\}. \quad (12)$$

4.1.4.1. Different methods.

As the roughness profile is discretised by the recording device, experimental points with exactly the same amplitude as the intercept are rarely obtained. More precisely, it is unusual to get the conditions $y_l = c$, $y_k = c$ and, consequently, an interpolation of experimental points must be implemented. Four methods can then be applied (Fig. 4) to interpolate intersection between intercept and profile:

- First method (L0) considers the upper point (x_l, y_l) of the profile for the beginning of the intercept and the lower point (x_k, y_k) for the end of the intercept (Fig. 4a). In mathematical terms this relation is given by

$$L_l = \begin{Bmatrix} (x_l, y_l), (x_k, y_k), x_k > x_l; y_l > c, y_{l-1} < c, y_k > c, \\ y_{k+1} < c, y_i > c; i \in [l+1..k-1]; L_l = x_k - x_l \end{Bmatrix}.$$
$$\quad (13)$$

- Second method (L1): From the two adjacent points (x_{l+1}, y_{l+1}) and (x_l, y_l) satisfying Eq. (13), the linear equation $\Delta' = a'x + b'$ is calculated, x_{left} is defined by $x_{\text{left}} = (c - b')/a'$. With the same method, x_{right} is obtained with (x_k, y_k) and (x_{k+1}, y_{k+1}) which gives $\Delta'' = a''x + b''$ with $x_{\text{right}} = (c-b'')/a''$ and finally $L_l = x_{\text{right}} - x_{\text{left}}$ (Fig. 4b).
- The third method (L2) could lead to better results. In method 2, to calculate the intersection between the profile and the value of the intercept, the Abbott curve was interpolated by a straight line (Fig. 4c). A more precise intersection can be found when (x_{i-1}, y_{i-1}), (x_i, y_i) and (x_{i+1}, y_{i+1}), with $y_{i-1} < y_i < c < y_{i+1}$, are interpolated by a parabola. To calculate the intersection, we first evaluate the equation $F(x) = ax^2 + bx + d$, the two roots of the equation $ax^2 + bx + d = c$ are calculated and the solution x_{left} is the root included in $[x_i, x_{i+1}]$. In the same way, the root x_{right} included in the interval $[x_j, x_{j+1}]$ is calculated with $[x_{j-1}, y_{j-1}]$, $[x_j, y_j]$ and $[x_{j+1}, y_{j+1}]$ with $y_{j-1} > y_j > c > y_{j+1}$.
- Fourth method (L3): In this method, (x_{i-2}, y_{i-2}), (x_{i-1}, y_{i-1}), (x_i, y_i) and (x_{i+1}, y_{i+1}), where $y_{i-2} < y_{i-1} < c < y_i < y_{i+1}$, are interpolated by a third-degree polynomial curve (Fig. 4d).

4.1.4.2. Analysis of the intercepted peak length.

At first, peak length error has to be analysed. For this purpose, different intercepted peak lengths estimated by the four methods are applied on the 800 experimental profiles described in Section 3. As the sampling length depends on the class of profiles, we shall normalise the error on the length determination in sampling length unit. With this unscaled unit, the error is bound to 2. In the same way, to normalise the influence of the profile amplitude on the peak length precision, the amplitude is divided by the range roughness. Then, we calculate the mean error for the four methods. The differences between the length obtained by method L3 (it is obvious that method L3 should be considered as the best one in terms of interpolation) and the others (L3−L0, L3−L1 and L3−L2) allow us to analyse the error for 20 normalised heights of intercept corresponding to all experimental profiles. This statistical technique was applied to analyse the bias on determining the length versus the height of intercept (in %). Then the error is plotted in sampling length units versus the height of the intercept (Fig. 5). As a matter of fact, the values obtained by method L3 are higher than those obtained by applying the method L0 for small intercept heights, and lower for higher intercepts. The biggest difference reaches 4% of the sampling length:
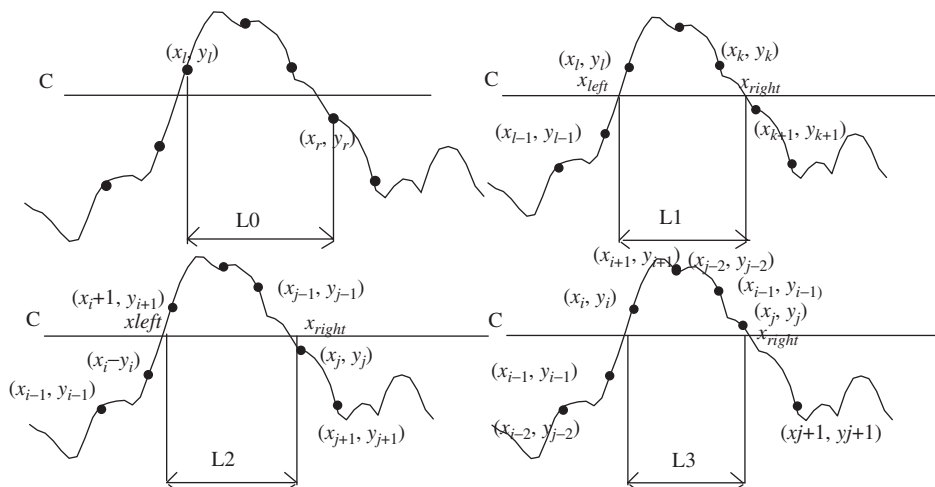

Fig. 4. Methods L0 (no profile interpolation), L1 (linear interpolation), L2 (parabolic interpolation) and L3 (third-degree polynomial interpolation) used to calculate the intercepted length.
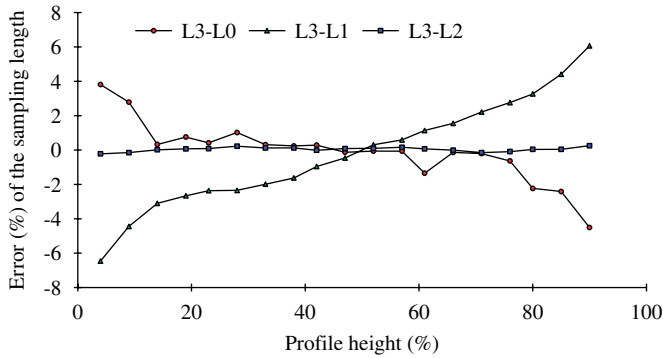
Fig. 5. Mean distribution error of peak length versus the relative height of profile for all experimental profiles described in Section 3. Each peak length for all the profiles is computed using the methods L0, L1, L2 and L3. Peak length is divided by the sampling length. Li3 is the error in percent of the sampling length obtained by the L3 method minus the intercepted length obtained with method Li. For these statistics, 216 550 peak lengths are calculated.

when a peak, or a valley, is defined with fewer than 5 points, method L0 underestimates the intercepted length for the valleys and on the contrary overestimates the intercepted length for the peaks. Method L1 gives worse precision than the L0 one. This surprising result can be explained by the analysis of the second order derivative of the profile $(\partial^2 y/\partial^2 x)$. In case of convexity $(\partial^2 y/\partial^2 x > 0)$, method L1 overestimates the intercepted length. If the profile possesses an inflection point $(\partial^2 y/\partial^2 x = 0)$, the error is minimal and corresponds to the value $y = 50\%$ for a high number of experimental profiles. In case of concavity $(\partial^2 y/\partial^2 x < 0)$, method L1 underestimates the intercepted length and method L2 gives better results. The main problem of the L2 interpolation is that the parabola and the profile intersection are not centred on the interpolation points. In fact, L2 minimises x_{left} and x_{right}. However, if we consider that a peak can be statistically symmetrical to its maximal value, the length $L = x_{\text{left}} - x_{\text{right}}$ should be centred on its true value. To verify this hypothesis, x_{left} and x_{right} are computed using both the L2 and L3 methods for 20 values of c on each peak of the 800 profiles. An analysis of variance shows that this difference does not depend on the intercept height. we obtain $x_{\text{left}}^{L3} - x_{\text{left}}^{L2} = 0.0297 \pm 0.0003$, $x_{\text{right}}^{L3} - x_{\text{right}}^{L2} = 0.0301 \pm 0.0003$ that gives a difference on the intercept length of $L^{L3} - L^{L2} = 0.0005 \pm 0.0003$. This difference is statistically insignificant, and therefore hypothesis (symmetrical peaks) is statistically confirmed. The conclusion from this analysis is that method L1 has to be proscribed and method L0 is appropriate if the optimisation of the computation time is searched rather than a better precision on the intercept length determination. Method L2 is more accurate when a better precision in the intercept length calculation is wanted. Finally, method L3 is required when the co-ordinates of the interception between profile and intercept have to be calculated for a particular roughness analysis.

4.1.5. t-Student computation

The $t_{x,k}$ calculation, used to estimate the confidence interval (Eq. (11)), needs complex integral with root research on integral functions. However, some approximate analytical formulae exist to estimate the t PDF and $t_{x,k}$ are found using a large series function with cosine terms that require much computational time. As the algorithm requires the computation of a high number of t PDF, an alternative approach consisting in approximating the t values, can be applied. As will be seen later, only one x value is required in our method. Consequently, $t_{x,k}$ was evaluated by a simple formula for one x and for any k: $t_{0.995,k}$ is approximated by the original following equation (Fig. 6):

$$t_{0.995,k} = 2.57 + 82.611e^{-1.18k-1.17} + 5.43/(k - 0.898). \quad (14)$$

The high confidence level of $1-\alpha = 0.995$ is justified: indeed when a high number of simulations is carried out, we are certain (in five cases out of 1000) that the estimated slope is included in the calculated confidence interval. If the usual statistical interval $1-\alpha = 0.95$ was used, five cases out of 100 would not be included in the confidence interval. As our algorithm leads to the calculation of over 1000 slopes, it is then possible to find a high number of slopes that would not be included in the confidence interval: consequently for different values of $_{1-\alpha}$, different ranges of the linear part of the Abbott curve are obtained. The lower the significant level $1-\alpha$, the higher the range of the linear part. To quantify experimentally the influence of the significant level on the determination of the Abbott parameters, the values of *Mr1* and *Mr2* are estimated from 10 electro-eroded profiles for different values of $1-\alpha$ (Fig. 7). As could be shown, the values of *Mr1* and *Mr2* (that affected all other Abbott parameters) are affected if $1-\alpha > 0.95$. As a consequence, the majored value of $1-\alpha = 0.995$ is retained for the determination of the linear part of the Abbott curves.

4.1.6. Minimal percentage on the Abbott curves

A small part of Abbott curves may present a good linear part that does not represent the central roughness amplitude. To avoid this artefact, the DIN norm proposes to take exactly 40% of the points to plot the linear part of the Abbott curve. *Is this value the best one*? To answer this question the Abbott parameters were calculated for all the profiles using L3 method with 200 intercepts by imposing the minimal range of AHD in the interval [5%, 95%] to estimate the precision on the amplitude coefficients (R_k, R_{vk} and R_{pk}). The precision on these coefficients depends on the precision in the determination of the slope of the linear part of the Abbott curve. The confidence interval of $F(x)$ at a point x_0 is given by

$$a + bx_0 \pm t_{1-\alpha/2, \atop n-2} s \sqrt{1 + 1/n + (x_0 - \bar{x})^2 / \sum_{i=1}^{n} (x_i - \bar{x})^2},$$
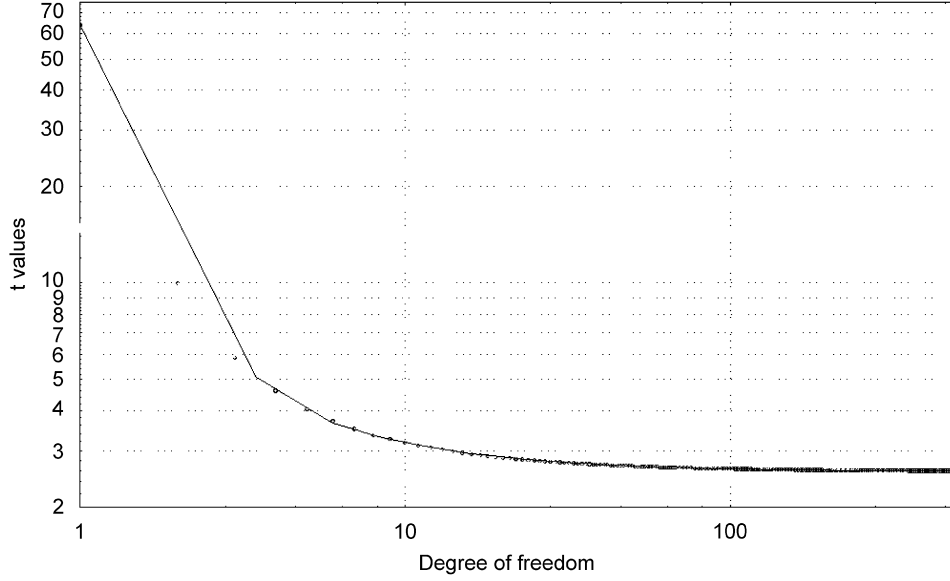
$$(15)$$

Fig. 6. Plot of $t_{0.995,k}$, Student's t value, versus degree of freedom (k). Full line corresponds to the non-linear regression given by Eq. (14).
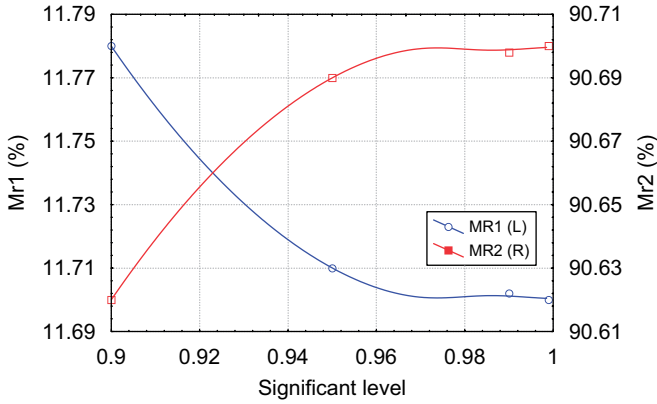

Fig. 7. Variation of Mr_1 and Mr_2 versus the significant level. The points reported on the graph correspond to the mean of the parameters calculated from 10 electro-eroded profiles (Fig. 2a).
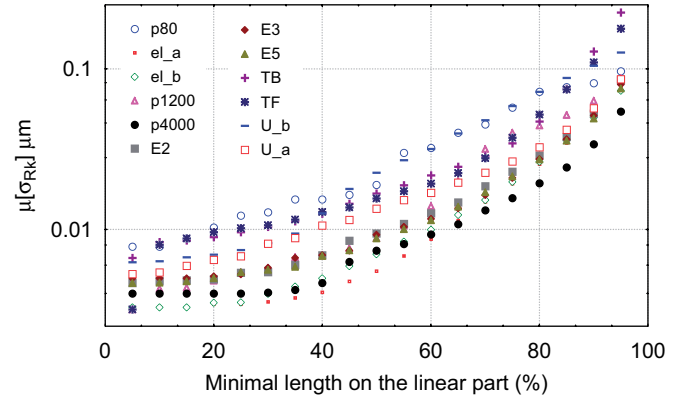

Fig. 8. Influence of the minimal length of the linear part on the mean for the R_k standard deviation for each class of experimental profiles described in Section 3.

where $\bar{x}$ is the mean of the n consecutive values of x_i included in the linear part.

Consequently, R_{vk}, R_k and R_{pk} standard deviations are, respectively, given by

$$\sigma_{R_{pk}} = s\sqrt{1 + \frac{1}{n} + \frac{(\bar{x})^2}{\sum_{i=1}^{n}(x_i - \bar{x})^2}},$$

$$\sigma_{R_{vk}} = s\sqrt{1 + \frac{1}{n} + \frac{(100 - \bar{x})^2}{\sum_{i=1}^{n}(x_i - \bar{x})^2}}, \quad \text{and}$$

$$\sigma_{R_k} \approx \frac{\sigma_{R_{vk}} + \sigma_{R_{pk}}}{2}. \tag{16}$$

These parameters can be considered as new roughness ones that characterise the disorder of the profiles. To analyse the effect of the minimal range of AHD, (AHD_{min}), profiles are normalised by dividing the profile height by the maximal range amplitude (R_t). Then for different values of

AHD_{min} (5–95% with an incremental step of 5%) and for each profile, σ_{Rk} was calculated, and finally the mean $\mu[\sigma_{Rk}]$ and the standard deviation $\sigma[\sigma_{Rk}]$ of σ_{Rk} were calculated for all profiles. It was found that the mean increases exponentially when AHD_{min} increases (Fig. 8) but is quite constant for AHD_{min} lower than 20%. As AHD_{min} increases, the probability that the straight line fits well with the Abbott curve decreases. Therefore, if the linear assumption is not respected, the probability of finding points of the Abbott curves far from the linear part rises, which will increase the standard deviation of $\sigma_{R_k}, \sigma_{R_{pk}}$ and $\sigma_{R_{vk}}$. However, taking the shortest AHD_{min} could lead to false results because of the presence of a short well-fitted linear part whose slope differs from the real linear Abbott domain. Consequently, AHD_{min} has also to minimise $\sigma[\sigma_{Rk}]$ for each category where $\sigma[\sigma_{Rk}]$ is minimal. As regards (Fig. 9), the Abbott parameters get good stability by taking a minimal range $\text{AHD}_{min} \approx 15\%$.

4.1.7. Intercept numbers on the Abbott curves

The number of intercepts (N) used to plot the Abbott curves influences the precision of the parameters since their true values are ideally obtained for an infinite number of intercepts. However, computational time increases with N and its choice must be optimised. *A1*, *A2*, *Mr1* and *Mr2* precision depends on the discretisation step length between two intercepts. For example, precision on *Mr1* or *Mr2* would not exceed $100/N$.

To evaluate N, two methods can be applied:

 (i) Creating an iterative algorithm to find the minimal number of intercepts that gives the precision on the parameters defining a norm and using a convergence criterion.
 (ii) Analysing convergence parameters on experimental profiles and finding the pertinent N.

The first method is the more efficient since no condition is imposed on the profile. However, increasing N increases the number of points of the Abbott curve and leads to a linear part with a high number of points. By a computation complexity study, it can be shown that an iterative algorithm increases time by eight times more than the deterministic one. For this reason, the iterative algorithm is left aside. We have analysed the influence of the number of intercepts used to plot the Abbott curves. All the profiles are computed with a number of intercepts included in the interval [20 … 500]. Then the means of the Abbott parameters for each group and the means of these means are computed. As *Mr1* and *Mr2* parameters determine totally the accuracy of the others, the variation of *Mr1* and *Mr2* are plotted versus the number of intercept lines (Fig. 10). It has to be noticed that after 250 points, the error on the determination of the parameters is lower than 2% for *Mr1* and lower than 0.1% for *Mr2*. The difference in accuracy between *Mr1* and *Mr2* is a consequence of the peak profiles' variations being more important than the valleys'. With the same analysis, it was proved that errors on R_{pk}, R_k and R_{vk} are less than 0.6% by taking 250
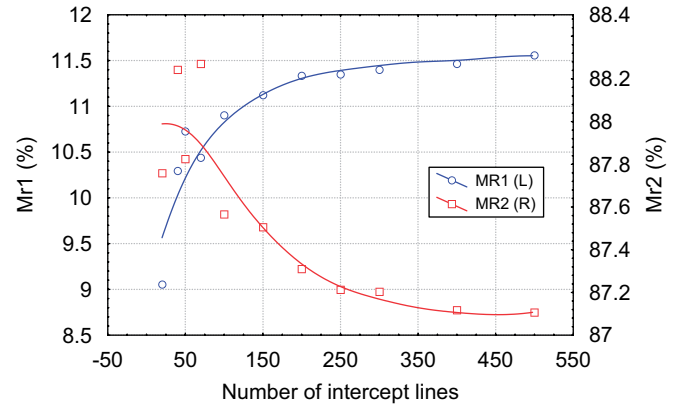

Fig. 10. *Mr1* and *Mr2* versus the number of intercepts. Points are means of *Mr1* and *Mr2* values for all experimental profiles described in Section 3.

intercept lines and errors on *A1* and *A2* do not exceed 1%. For these reasons, all the Abbott curves will be plotted with 250 intercepts.

4.2. The extended Abbott parameters

As in the DIN norm the Abbott parameters are defined for sigmoid curves, some errors may appear when parameters are computed on non-sigmoidal ones. Two possibilities can then be considered to avoid eventual artefacts. Firstly, when the computed parameters do not respect rigorously the DIN norm specification, the parameters will not be performed. Secondly, the DIN norm is modified to calculate all the parameters for the non-sigmoidal curves, and to obtain the same values as the norm states for sigmoidal ones. For example, if we analyse the Abbott curve of a sinusoidal profile, no DIN parameter can be computed (Fig. 11). Let us analyse the physical meaning of the R_{pk}: this parameter was created to represent the mean height of peaks that passes over the distribution of the "peaks of the interior profile" and then to characterise some physical surface properties like the wear processes. For the sinusoidal profile, no peak exists over the interior profile. Consequently, the DIN norm could present this major defect when Abbott parameters are used to quantify the effect of a physical process on the modification of the surface topography: suppose that a wear phenomenon has to be characterised by the modification of the surface topography during wear cycles. On the initial surface, Abbott parameters are computed respecting the DIN norm. Then the wear process erodes the peaks at each wear cycle that will decrease the R_{PK} value. During the wear process, it may happen that peaks are too eroded to be characterised by the R_{PK} with respect to the DIN norm. As a consequence, the wear damage can only be characterised by the Abbott parameters on a reduced time interval. This example proved that the DIN norm has to be extended under the following assumptions:

 (i) respect the DIN philosophy,
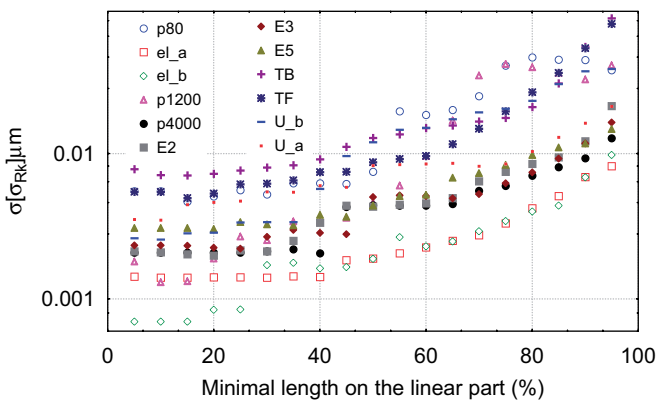 (ii) parameters can always be computed,

Fig. 9. Influence of the minimal length of the linear part on the standard deviation for the R_k standard deviation for each class of experimental profiles described in Section 3.

(iii) give exactly the same parameter values as the DIN norm if Abbott curves are sigmoidal,

(iv) the values of all parameters have to be numerically continuous in the transition [calculable by the DIN norm—non-calculable by the DIN norm],

(v) looking at Abbott parameters, experimenters must be able to conclude if the parameters tally with the DIN norm or are extended DIN parameters.

For example, let us analyse the parameter *Mr1* (Fig. 11) of the Abbott curve applied to a noisy sinusoidal profile. To be computed by the DIN norm, the Abbott curve must lie above the regression line. *Mr1* equals zero if the regression line and the Abbott curve are superposed. If the Abbott curve is under the regression line, then *Mr1* cannot

Fig. 11. Calculus of the modified Abbott parameters on a non-sigmoidal Abbott curve.

be computed. However, let *Mr1* be the value of the intersection between the highest point of the Abbott curve and the regression line, then *A1* becomes the area between the highest point and the Abbott curve. This area becomes negative and characterises an excessive wear of the peak. It becomes obvious that this parameter is continuous and no discontinuity appears in the transition $A1 = 0$. The same method is applied for *A2* computation.

4.3. Experimental profiles

In this part, Abbott and extended Abbott parameters are computed to analyse the modification of surface topography due to different physical processes.

4.3.1. Electro-erosion

Does pulse time duration have an influence on surface roughness? To answer this question, the Abbott parameters were computed for different profiles (Fig. 12). By analysis of variance, it can be remarked that R_{pk}, R_k, R_{vk}, *A1* are highly discriminating for the electro-erosion process. On the contrary, *Mr1*, *Mr2* and *A2* do not allow us to discriminate it. To normalise these parameters, we decided to reduce each Abbott curve by dividing R_{pk}, R_k and R_{vk} by R_t (with $R_t = R_{pk} + R_k + R_{vk}$) to obtain the reduced coefficients R_{pk}^*, R_k^* and R_{vk}^* (Table 2). A new analysis of variance led us to conclude that $R_{pk_{el\_a}}^* = R_{pk_{el\_b}}^*$, $R_{k_{el\_a}}^* = R_{k_{el\_b}}^*$ and $R_{vk_{el\_a}}^* = R_{vk_{el\_b}}^*$. That means that peaks and valleys get the same morphology. As *Mr1* and *Mr2* do not depend on the scale unit and as it was proved by
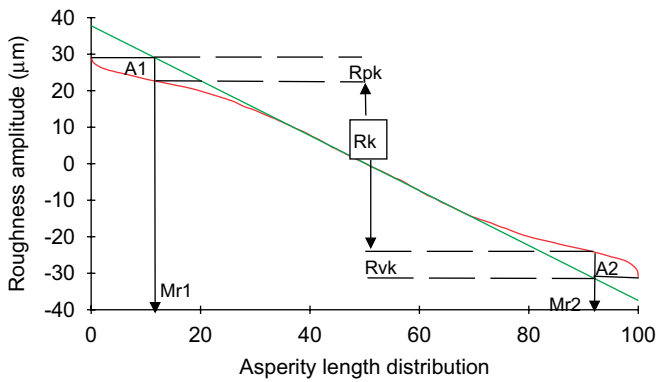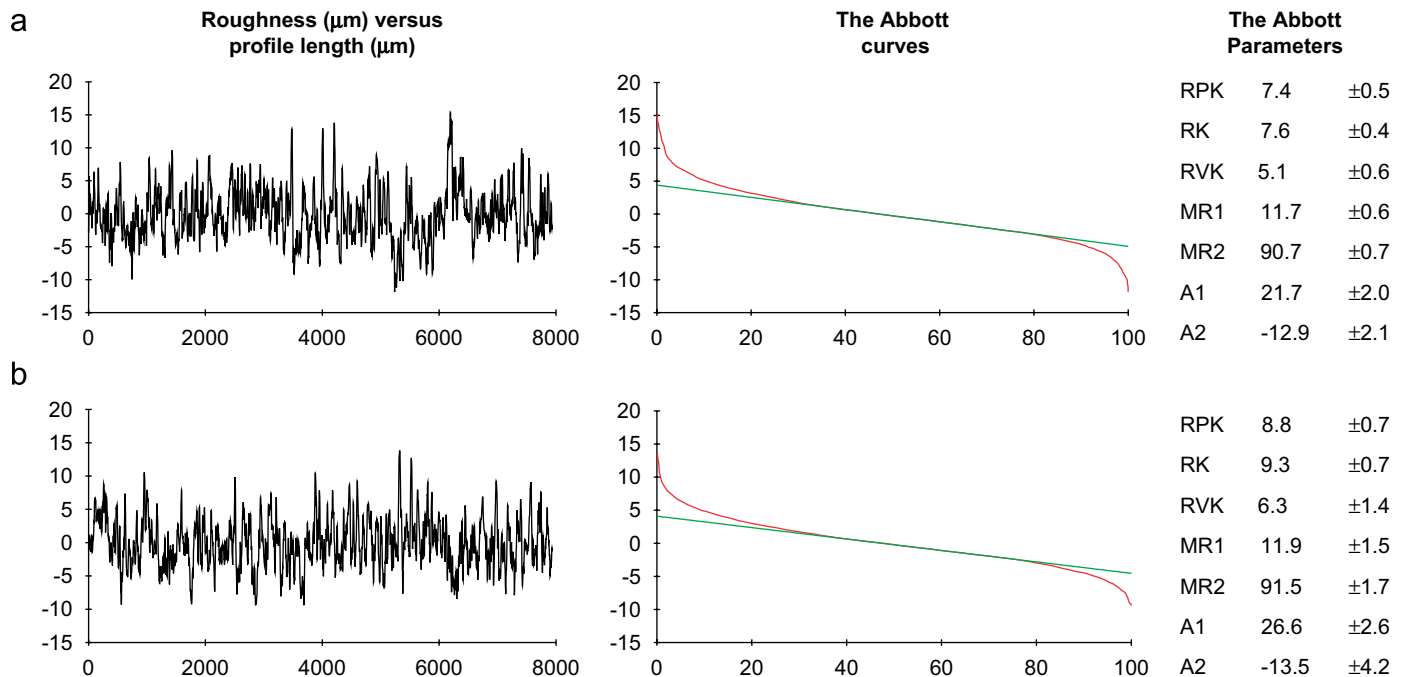

Fig. 12. Abbott parameter computation on two different electro-eroded profiles. Thirty profiles are measured and Abbott statistical parameters are computed. Pulse time duration is 1.5 ms for sample A (a) and 2.5 ms for sample B (b).

the statistical analysis that amplitude structure is scale independent, then electro-erosion profiles are statistically self-affine, describing a fractal structure.

4.3.2. Turning

All the Abbott parameters characterise the feed rate parameters (Fig. 13). When the feed rate increases, all parameters that characterise peaks increase except for R_{vk}. Increasing the feed rate from 0.1 mm/rpm (Fig. 13a) to 0.35 mm/rpm (Fig. 13b) increases the roughness amplitude ($R_{pk_{U\_a}} + R_{k_{U\_a}} + R_{vk_{U\_a}} = 21.5\,\mu\text{m}$, $R_{pk_{U\_b}} + R_{k_{U\_b}} + R_{vk_{U\_b}} = 28.8\,\mu\text{m}$). As shown earlier (Section 4.3.1), the amplitude roughness parameters were

standardised (Table 2). We can conclude that decreasing the feed rate decreases the peak amplitude due to friction between the material and the turning tool. The material is snatched away for small feed rates and is peeled off for higher ones. The values of $Mr1$ confirm this hypothesis ($Mr1_{U\_a} = 6.5$, $Mr1_{U\_b} = 18.2$) as the most important volume of peaks for the profiles U_b ($A1_{U\_a} = 2.5$, $A1_{U\_b} = 81.9$).

4.3.3. Shot peening

By analysing variance, it can be shown that all the parameters discriminate among the different samples except for $Mr1$ (Fig. 14). Those experimental profiles are

Table 2
Values of reduced Abbott amplitude parameters

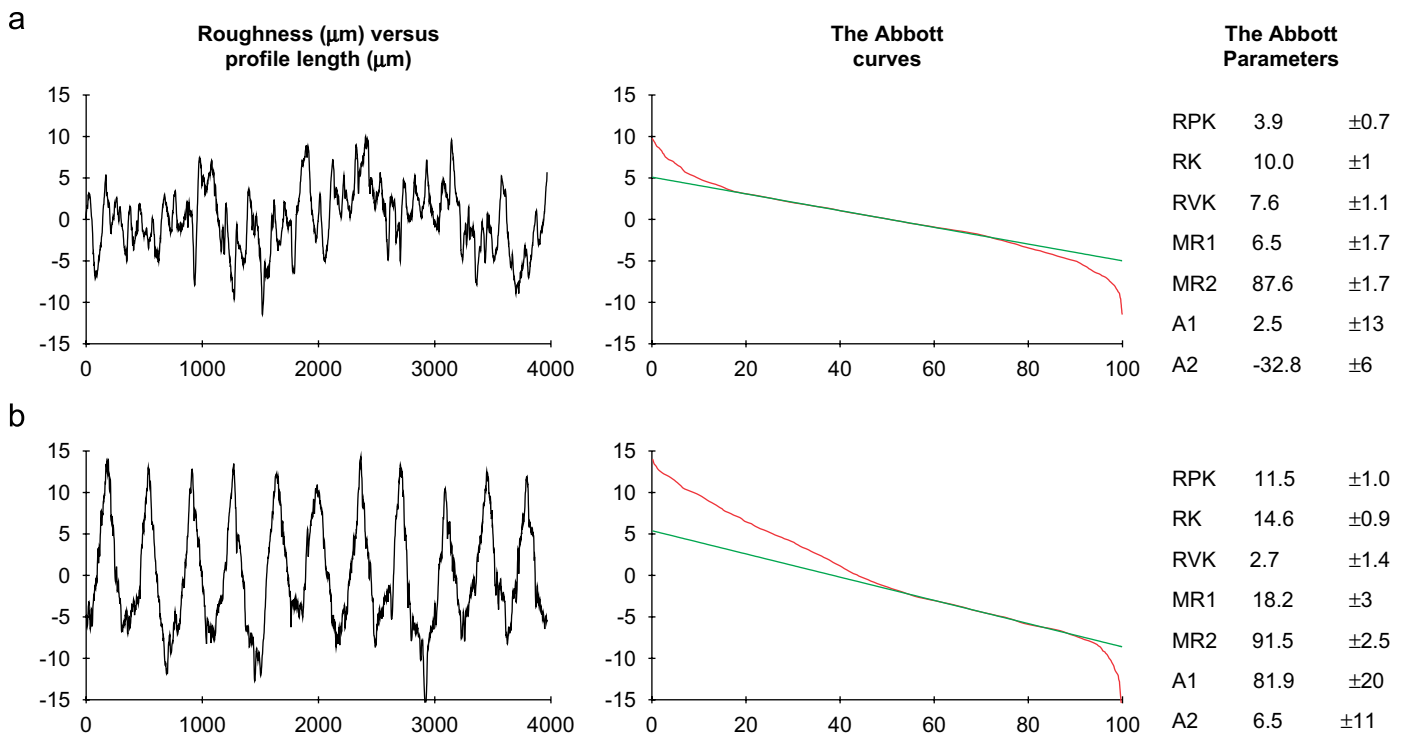| Study	R_{pk}^* (%)			R_k^*			R_{vk}^*		
Electro-erosion	el_a	el_b		el_a	el_b		el_a	el_b	
	37	36		38	38		25	26	
Tool machine milling	U_a	U_b		U_a	U_b		U_a	U_b	
	18	40		46	50		36	10	
Shot penning	E2	E3	E5	E2	E3	E5	E2	E3	E5
	23	29	26	47	41	34	30	40	40
Wear of hip prothesis head	TB		TF	TB		TF	TB		TF
	8		36	30		21	62		9

Fig. 13. The Abbott parameter computation on two different tool-machined profiles (2×30 profiles). (a) and (b) are machined, respectively, with an advanced sample of 0.1 and 0.3 mm/rpm.

quite satisfactory as far as the fractal structure is concerned. If we use the reduced amplitude Abbott parameters, it can be concluded that profiles E5, before shot peening, get the same parameters as the E3 ones after shot peening in dry environment (Table 2). It could statistically be proved by Student's test that $R^*_{pk_{E3}} \approx R^*_{pk_{E5}}$, $R^*_{k_{E3}} \approx R^*_{k_{E5}}$, $R^*_{vk_{E3}} \approx R^*_{vk_{E5}}$, $Mr1^*_{E3} \approx Mr1^*_{E5}$ and $Mr2^*_{E3} \approx Mr2^*_{E5}$. This clearly means that shot peening in dry environment does not affect the mass peak distribution. However, profiles E5 present a more disordered aspect. This example proves that Abbott parameters do not characterise the frequency feature of the profile (like the usual roughness amplitude coefficient Ra).

4.3.4. Wear of hip prosthesis head

Firstly, the worn surface of the prosthesis head gets quite a higher amplitude than the unworn one ($R_{pk} + R_k + R_{vk} = 5.49\,\mu m$ against $6.78\,\mu m$) (Fig. 15). The main aspect is the difference between the percentage of valleys for the more solicited part (TF) and the less solicited one (TB). The central roughness amplitude is not large

(Table 2). This analysis is confirmed by the values of $Mr1$ and $Mr2$ ($Mr1_{TB} = 7.5$, $Mr1_{TF} = 23.5$ and $Mr2_{TB} = 80.7$, $Mr2_{TF} = 91.3$). As regards these values, profiles TB and TF seem to be inverted in amplitude. An analysis of the wear mechanisms shows that the wear surface TF is damaged by a TA6V fibre between the hip prosthesis and the cup. Biomedical and chemical investigations show that fibre moves (when the human body does) without constraint in the TB region and is immobilised in the constraint zone (TF) during an undetermined period. This hypothesis seems to be confirmed by this study of roughness parameters: immobilised fibre creates important valleys and then the linear part of the Abbott curves is displaced into the peak zone.

4.3.5. Polished surface

It may be logical to find a statistical self-affinity fractal structure because the abrasive grains get the same morphology (Fig. 16). By this fact, the same values of the reduced amplitude Abbott parameters are expected. However, this fact is not confirmed by the experimental values and could
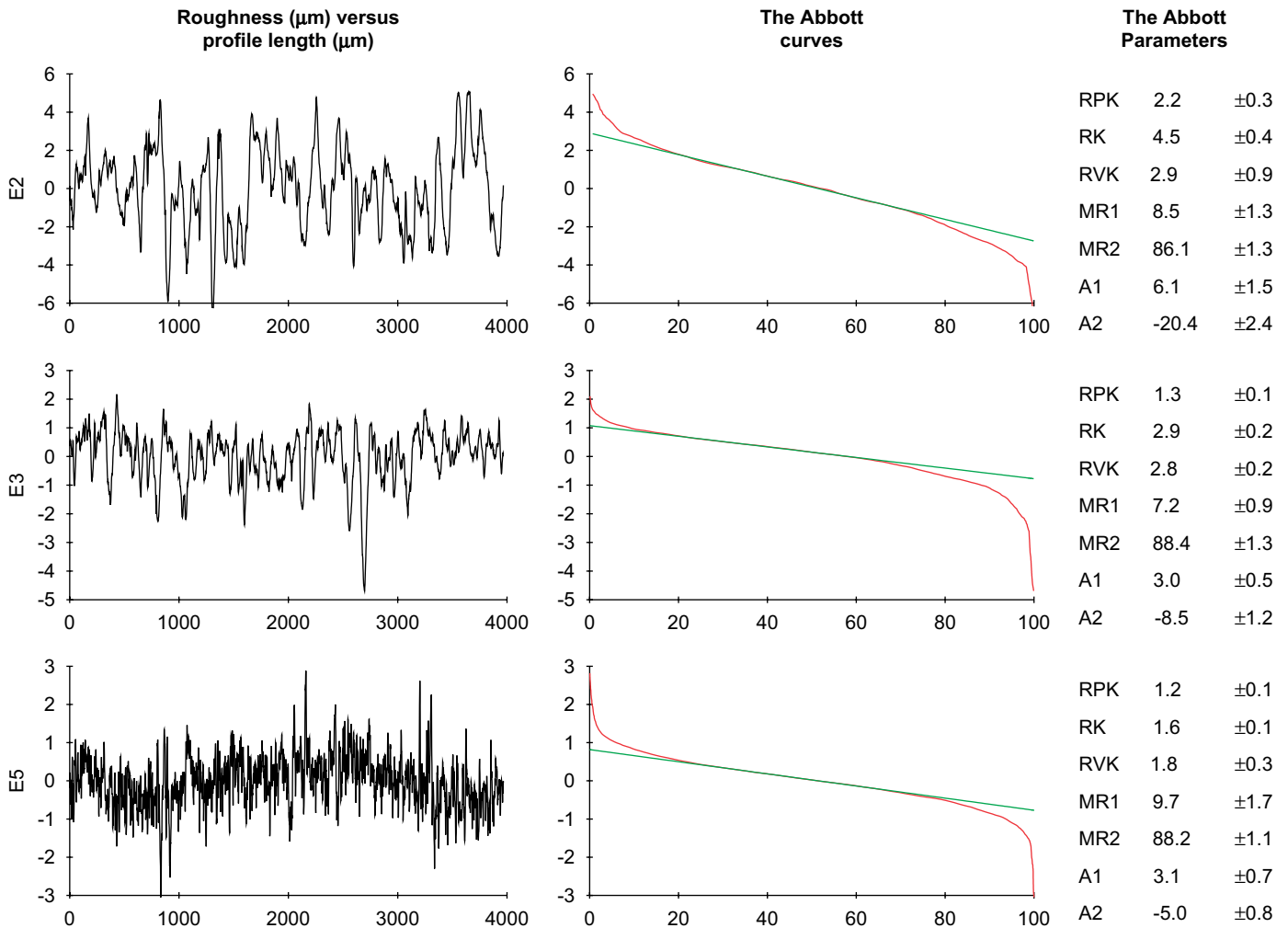

Fig. 14. The computation of the Abbott parameters for two different shot peening surfaces (E2, E3) and the original one before shot peening (E5) (3×30 profiles).

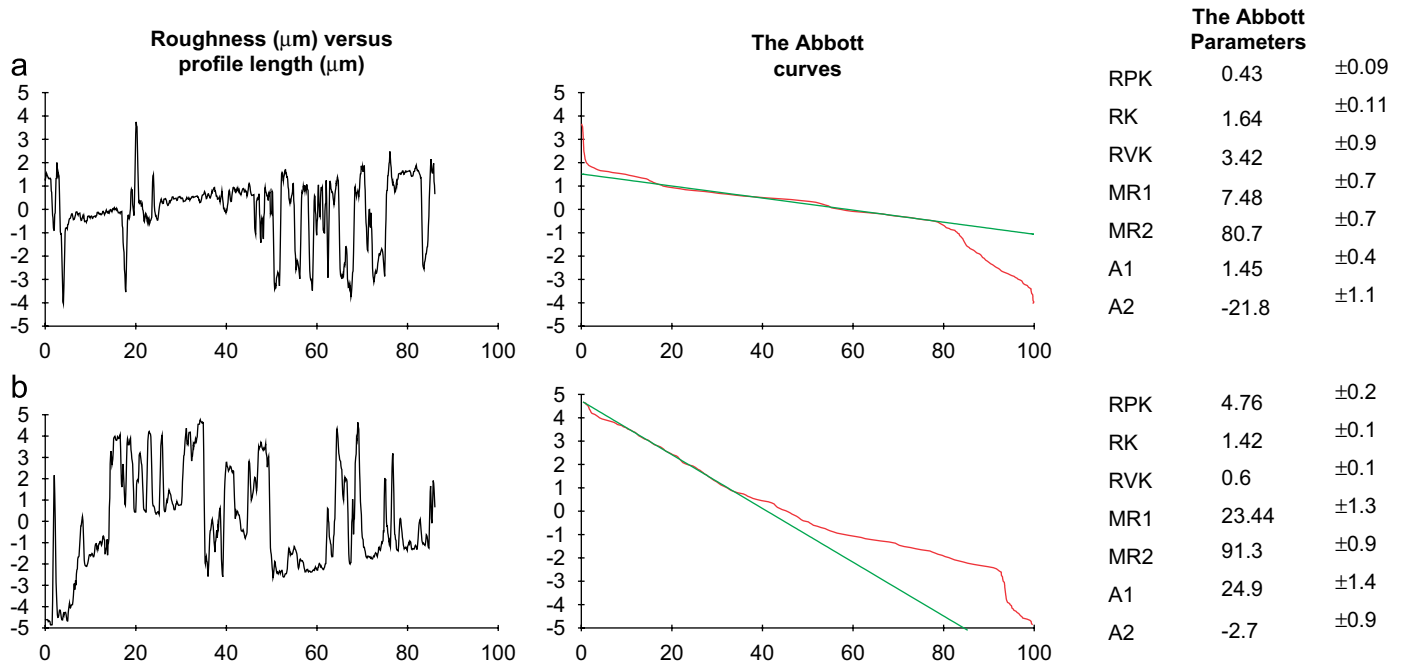|	**The Abbott Parameters**	
RPK	0.43	±0.09
RK	1.64	±0.11
RVK	3.42	±0.9
MR1	7.48	±0.7
MR2	80.7	±0.7
A1	1.45	±0.4
A2	-21.8	±1.1
RPK	4.76	±0.2
RK	1.42	±0.1
RVK	0.6	±0.1
MR1	23.44	±1.3
MR2	91.3	±0.9
A1	24.9	±1.4
A2	-2.7	±0.9

Fig. 15. The computation of the Abbott parameters for two different parts of a TA6V prosthesis head (280 profiles). (a) Represent the less damaged surface (TB) and (b) the more damaged one (TF).

be explained by the difficulty in evaluating the intercept length when the number of intercepts is decreasing.

4.4. Simulated profiles

To validate the efficiency of our algorithm, different categories of profiles were simulated. As analytical functions are not stochastic and lead to identical results (that do not allow us to validate our algorithm), a stochastic fractal profile was added to the original non-stochastic ones to obtain global stochastic ones. To simulate consequent profiles that look like experimental ones, we choose the Weierstrass–Mandelbrot function [9] (Fig. 17a). Six categories of profiles were simulated on purpose to represent most of the profiles met in surface analyses (Fig. 17b–g). One hundred profiles were simulated, the related Abbott parameters were calculated by our algorithm and finally descriptive statistics were computed.

The profile (a) presents a sigmoidal Abbott curve on which the DIN norm is applied without any restriction. All values are positive except for *A2* meaning that the area is calculated under the straight line.

The Profile (b) shows an Abbott curve on which only extended DIN parameters can be computed. As a result, *A1*, *A2*, R_{pk}, R_{vk} get opposite signs because the Abbott curve is under the straight line on the left and above on the right.

Profiles (c) and (d) represent, respectively, a half-sigmoidal curve and inverted one, then R_{pk} and R_{vk} get opposite signs. The range [*Mr1*, *Mr2*] is located on the upper profile height for (d) and in lower profile for (c).

Profile (e) represents a sigmoidal profile with small *A1* and *A2*. If no fractal noise is introduced in this triangular

profile, *A1* = *A2* = 0 and Abbott curves will be straight lines. In this case, *A1* and *A2* are a measure of the fractal noise.

For profiles (f) and (g), the slopes of the Abbott curves are calculated from valley (f) and from peak (g) for two reasons:

(i) peaks or valleys get large amplitude when compared with the fractal amplitude function,
(ii) peaks or valleys get less variance in a statistical sense than the fractal noise: points are aligned in the Abbott graph in which regression is computed.

In this case, Abbott curves formally have to be decomposed in two parts that represent macro and micro roughness, and the cut-off between these two stages could lead to new Abbott parameter definitions (micro and macro). Using these publication results, a new definition of parameters characterising the two stages will emerge.

4.5. Wear analysis

The method developed before also has to be validated on a dynamic physical process. In this part, we first simulated a wear model, applied it to the curves (a)–(f) of Fig. 17 and then analysed the evolution of the wear process through the evolution of the Abbott parameters.

4.5.1. Wear simulation

The following elementary model is used to simulate a wear process. Let $W(x)$, be the probability that a wear phenomenon erodes an element with height *dh* during each

Roughness (μm) versus profile length (μm)

The Abbott curves

	The Abbott Parameters	
RPK	1.7	±0.7
RK	2.8	±0.6
RVK	1.7	±0.6
MR1	12.1	±4.7
MR2	85.1	±7
A1	7.8	±4
A2	-12.1	±12

RPK	0.48	±0.16
RK	0.34	±0.07
RVK	0.45	±0.1
MR1	11.5	±1.7
MR2	82	±6.4
A1	1.34	±0.7
A2	-2.8	±1.8

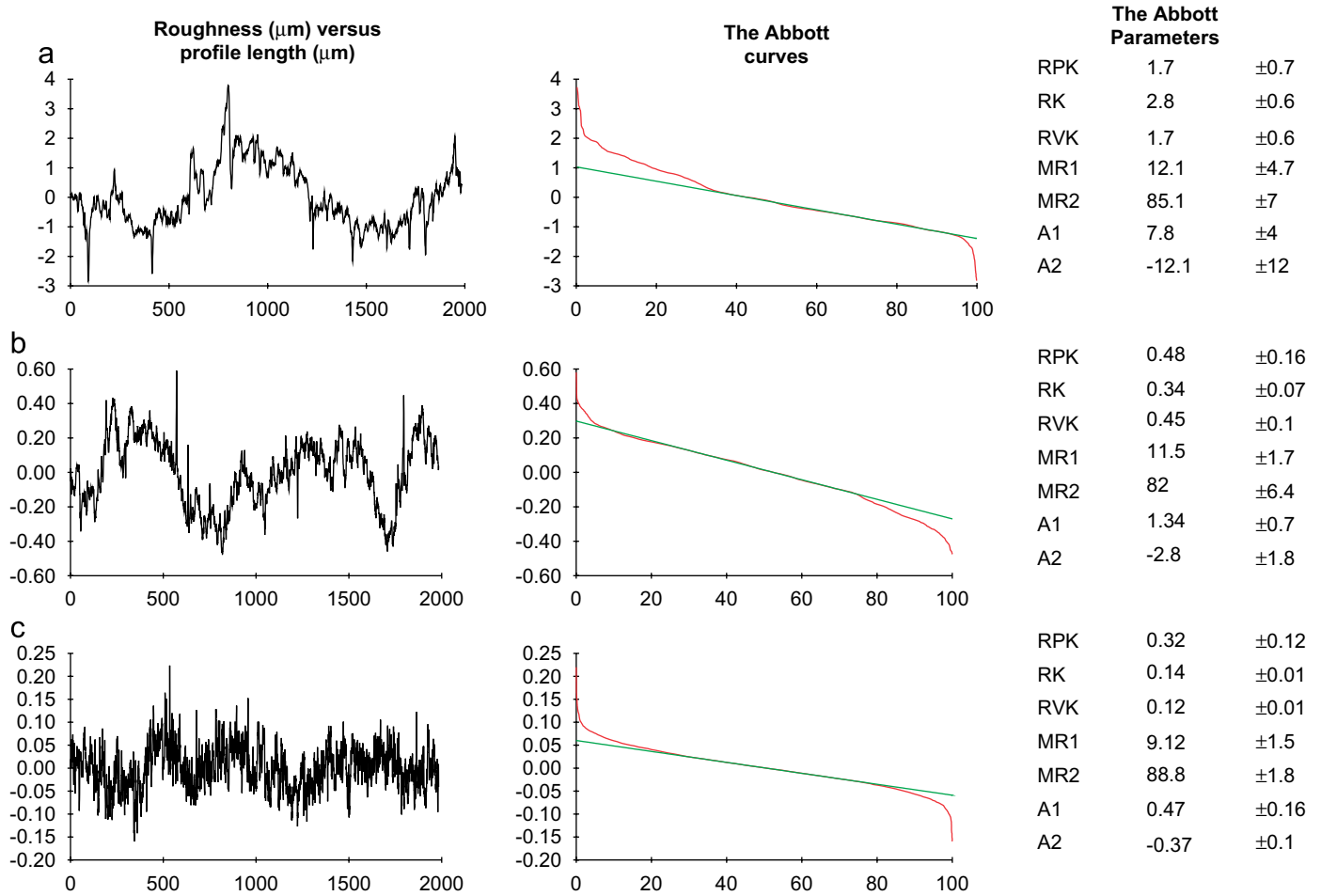|		
RPK	0.32	±0.12
RK	0.14	±0.01
RVK	0.12	±0.01
MR1	9.12	±1.5
MR2	88.8	±1.8
A1	0.47	±0.16
A2	-0.37	±0.1

Fig. 16. The computation of the Abbott parameters for three different polished surfaces (30 profiles). Surfaces are, respectively, polished with paper 80 (a), 1200 (b) and 4000 (c).

wear cycle (the higher the *dh*, the less wear resistant the material). Let Z_{max} be the maximal height of the profile and Z_{min} the minimal one. As the wear process does not erode materials on a depth lower than Z_{min}, we defined the probability to erode an elementary volume of the material during every wear cycle by

$$W(x) = k \int_0^{Z_{max}-z} e^{-\lambda x}\, dx, \qquad (17)$$

where k and λ are real numbers. The higher the λ, the higher the wear phenomenae (intensity stress, corrosion and so on). This trivial model can be applied only on regular profiles without auto-correlation. Wear integral (Eq. (17)) is normalised to obtain a PDF, then $k \int_0^{Z_{max}-Z_{min}} e^{-\lambda x}\, dx = 1$ and the following expression can be deduced:

$$k = \left[(1 - e^{-\lambda(Z_{max}-z)})/\lambda \right]^{-1}. \qquad (18)$$

The probability that an elementary material volume can be eroded at a height z is finally given by

$$W(x) = 1 - k\left(1 - e^{-\lambda(Z_{max}-z)}\right). \qquad (19)$$

4.5.2. Wear results

Wear algorithm is applied to curves presented in Fig. 17. With parameters $\lambda = 0.1$ and $dh = 0.01$. For every 100 wear cycles, the Abbott parameters are computed up to 2000 cycles. The profile and the associated Abbott curves are represented at the end of the wear process in Fig. 18. During the wear process *A1* decreases, i.e. peaks are eroded by the wear phenomenon. *A1* is positive for fewer than 900 wear cycles and becomes negative after (Fig. 18d). As was stated in section 4.2, the transition from the DIN parameters to the extended DIN ones respects continuity.

4.6. Manual-computer comparison

Generally, the Abbott parameters are manually calculated and the main difficulty consists in drawing the slope of the Abbott curves and determining *Mr1* and *Mr2*. In this part, we shall compare the manual and the computation methods.

4.6.1. Methodology comparison

Sixty profiles were recorded by a tactile profilometer on an electro-eroded surface discussed in Section 3.1 (Fig. 2a)
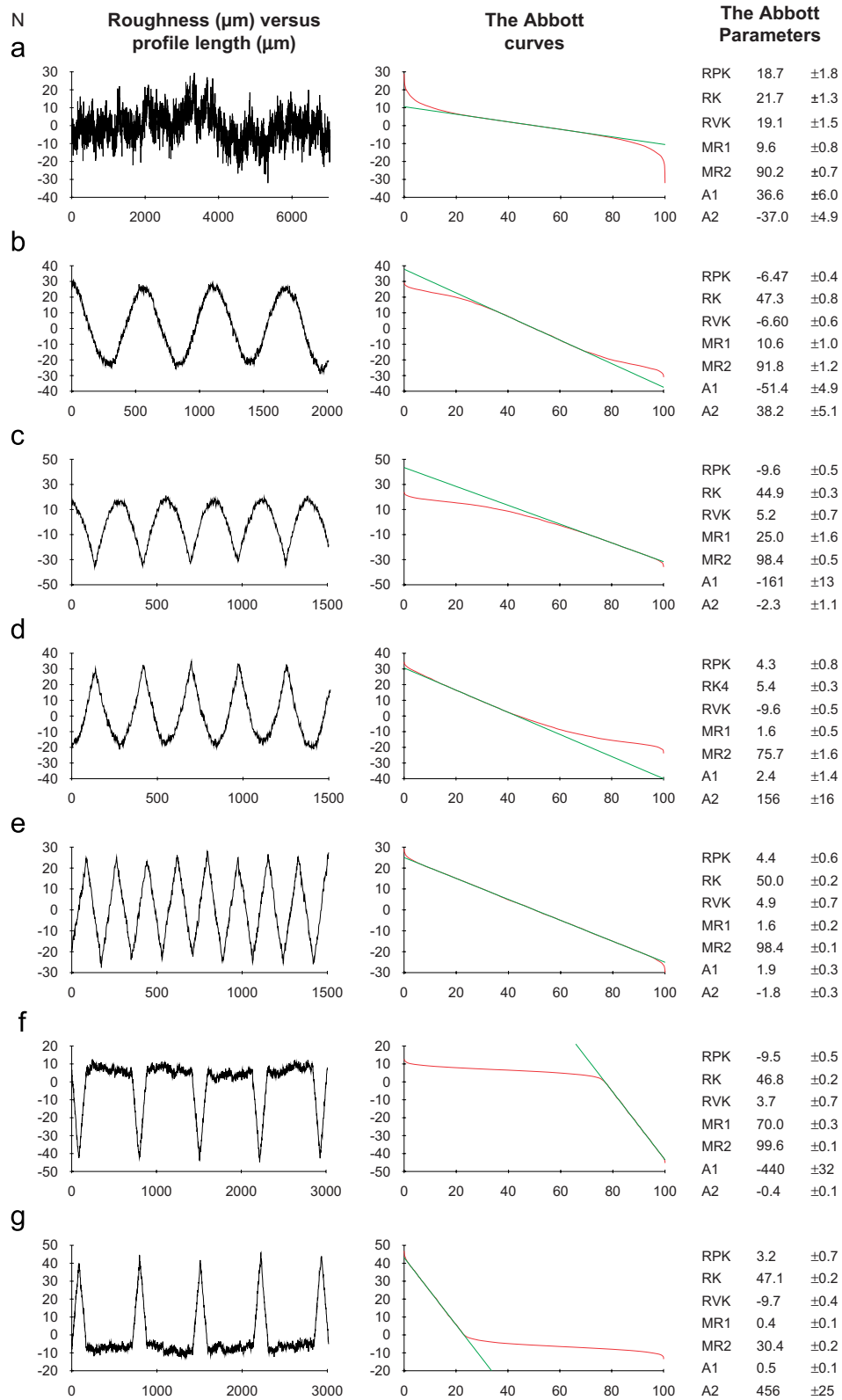
Fig. 17. Abbott parameters computation on different kinds of profiles. Hundred Fractal functions are computed (a), reduced in amplitude and added to a sinusoid (b), half-sinusoid (c and d), triangular function (e), "cracked" function (f) and "peaked" functions (g).

where the Abbott curves are sigmoidal. Then three evaluations were carried out on all the profiles by different experimenters to determine the Abbott parameters. We retained only the *Mr1* and *Mr2* estimations since the precision on the other Abbott parameters mainly depends on the determination of these two parameters.
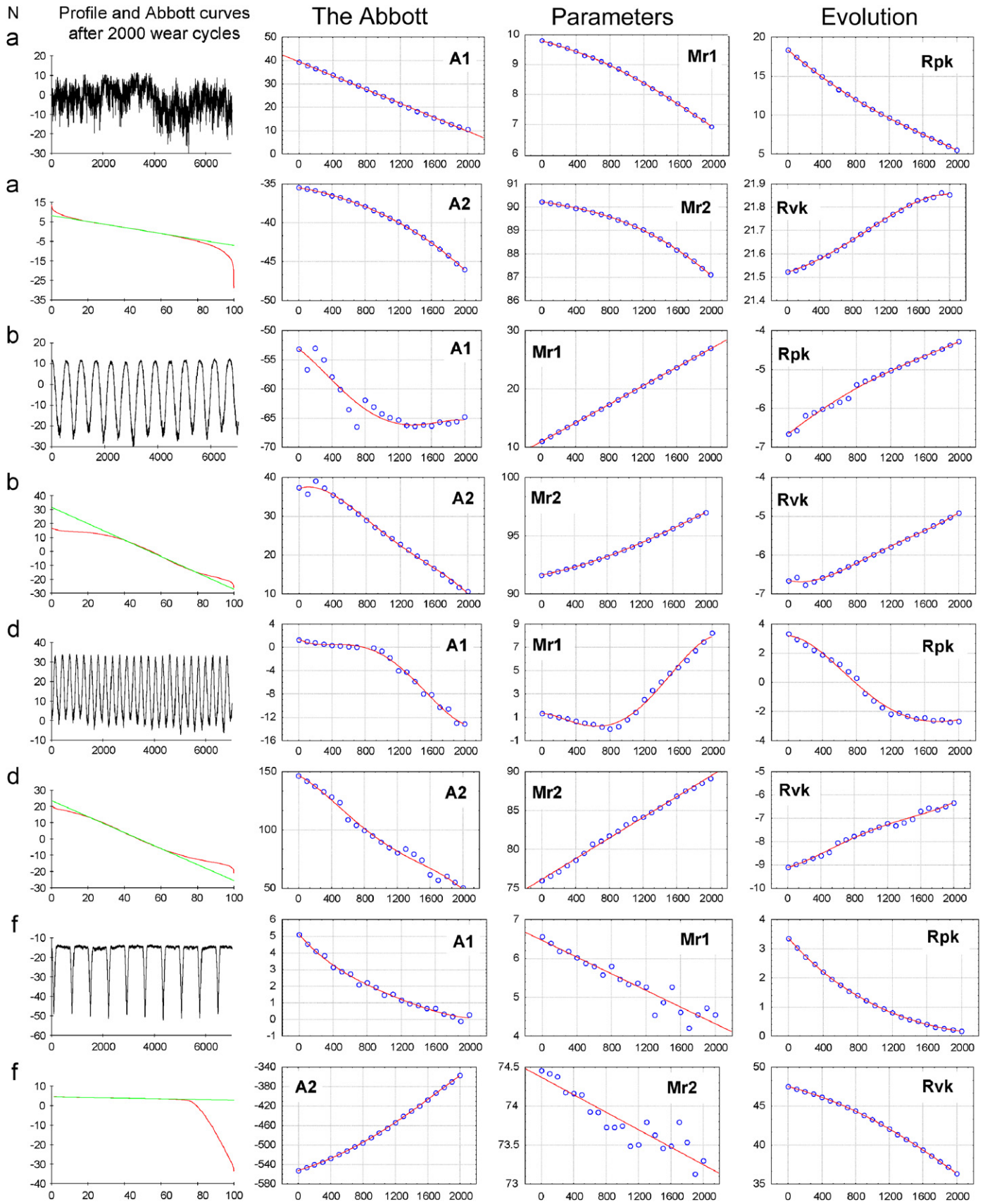
Fig. 18. Profiles and Abbott curves after 2000 wear cycles applied on original profiles of Fig. 17.

Table 3
Comparison between manual and the computed methods to calculate *Mr1* and *Mr 2* parameters on 60 profiles of electro-eroded surface (Fig. 2)

Parameter	Determination methods	Mean	Median	Minimum	Maximum	Standard deviation
Mr1	Manual	11.98	11.95	7.06	16.30	2.24
Mr1	Algorithm	11.36	11.63	6.04	14.94	1.85
Mr2	Manual	89.82	89.94	83.42	96.19	2.37
Mr2	Algorithm	90.86	90.94	85.96	94.72	1.72

4.6.2. Results from comparison

Statistical results are reported in Table 3. Both *Mr1* PDF (manual and automatic) obey a Gaussian law (critical values of the Shapiro Wilks test on manual determination: 0.1497, automatic: 0.1352). *Mr2* also obeys a Gaussian PDF for both methods (manual: 0.97, automatic: 0.98). Both automatic *Mr1* and *Mr2* determinations are higher than manual ones: experimenters unconsciously minimise the range of the linear part of the Abbott curves that lead to a lower range for $F(x)$ equation given by the algorithm. The dispersion is higher if the parameters are evaluated manually without any computation. However, the difference between manual and automatic evaluations is less than 1%. As a result our algorithm is reliable and could accurately be applied to experimental profiles.

5. Conclusion

An algorithm was performed in order to have an automatic evaluation of the Abbott curve parameters. Execution time does not exceed 0.1 s on a personal computer. Discretisation artefacts are discussed by analysing experimental and theoretical profiles, and lead to the conclusion that parameter estimations are accurate. As a high number of different profiles were accurately analysed, we think that our algorithm can be applied to a high number of experimental profiles. Like all numerical techniques, some particular profiles could lead to erroneous results (high isolated peak, or valley, non-stationary profiles, micro and macro-roughness, etc.). However, the Abbott curves have no application in those typical cases and another parameters will be more appropriate to characterise such types of profiles. It was shown that fractal functions could be used to simulate a wear process or to validate the efficiency of the parameter. This method

was applied for over 3 years in our laboratory and nothing outrageous was found moreover it can be extended to 3D surfaces [10] without any problem. Finally, some algorithms and results described in this paper will be helpful to calculate other roughness parameters such as the number of peaks, the radius of curvature and so on.

References

[1] Abbott EJ, Firestone FA. Specifying surface quality. Mech Eng 1933;59:569–72.
[2] Torrance AA. A simple datum for measurement of the Abbott curve of a profile and its first derivative. Tribol Int 1997;30(3):239–44.
[3] Malburg MC, Raja J. Characterization of surface texture generated by plateau honing process. Ann CIRP 1993;42:637–9.
[4] Deutsche Normen, Kenngrössen R_k, R_{pk}, R_{vk}, M_{r1}, M_{r2} zur Beschreibung des Materialanteils im Rauheitsprofil. Messung der profiltiefe Pt von Oberflächen, DIN 4776, Berlin, Mai 1990.
[5] NF ISO 13565. AFNOR, Paris, 1995.
[6] Lacey P, Torrance AA, Fitzpatrick JA. The relation between the friction of lubricated surfaces and apparent normal pressure. ASME J Tribol 1989;111:260–4.
[7] Lacey P, Torrance AA. The calculation of wear coefficients for plastic contacts. Wear 1991;145:367–83.
[8] Gruber MHJ. Regression estimators, a comparative study, in statistical modeling and decision science. Boston: Academic Press Inc.; 1990.
[9] Ganti S, Bhushan B. Generalized fractal analysis and its applications to engineering surfaces. Wear 1995;180:17–34.
[10] Dong WP, Sullivan PJ, Stout KJ. Comprehensive study of parameters for characterizing three dimensional surface topography. III parameters for characterizing amplitude and some functional properties. Wear 1994;178:29–43.